Stem Cell Reports, Volume *17*

Supplemental Information

The blood-brain barrier is dysregulated in COVID-19 and serves as a CNS entry route for SARS-CoV-2

Susanne Krasemann, Undine Haferkamp, Susanne Pfefferle, Marcel S. Woo, Fabian Heinrich, Michaela Schweizer, Antje Appelt-Menzel, Alevtina Cubukova, Janica Barenberg, Jennifer Leu, Kristin Hartmann, Edda Thies, Jessica Lisa Littau, Diego Sepulveda-Falla, Liang Zhang, Kathy Ton, Yan Liang, Jakob Matschke, Franz Ricklefs, Thomas Sauvigny, Jan Sperhake, Antonia Fitzek, Anna Gerhartl, Andreas Brachner, Nina Geiger, Eva-Maria König, Jochen Bodem, Sören Franzenburg, Andre Franke, Stefan Moese, Franz-Josef Müller, Gerd Geisslinger, Carsten Claussen, Aimo Kannt, Andrea Zaliani, Philip Gribbon, Benjamin Ondruschka, Winfried Neuhaus, Manuel A. Friese, Markus Glatzel, and Ole Pless

Supplemental information

Supplemental figures and legends

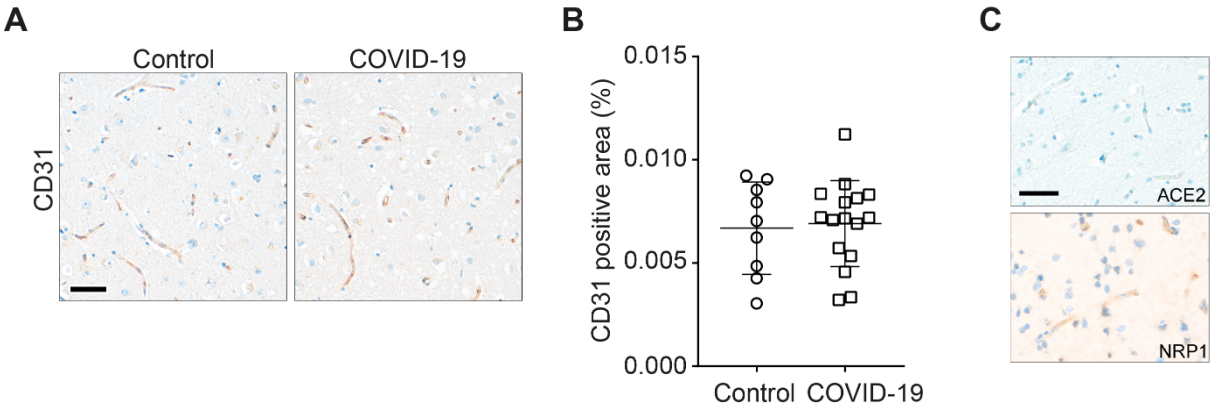

SI Figure 1: Expression of CD31 is not altered in COVID-19 brains and control brains express ACE2 and NRP1 in the vasculature. (A) Representative images of immune-histochemical staining for CD31 (brown) in control or COVID-19 human cortex brain tissue. No differences in expression can be observed. Scale bar: 50 μM. **(B)** Quantification of the signal as in (A) of CD31-positive area (%) in COVID-19 vs. control cortex tissue confirmed that CD31 expression is not altered in fatal SARS-CoV-2 infection. **(C)** Representative images of ACE2 and NRP1 expression in human cortex brain tissue. Scale bar: 50 μm.

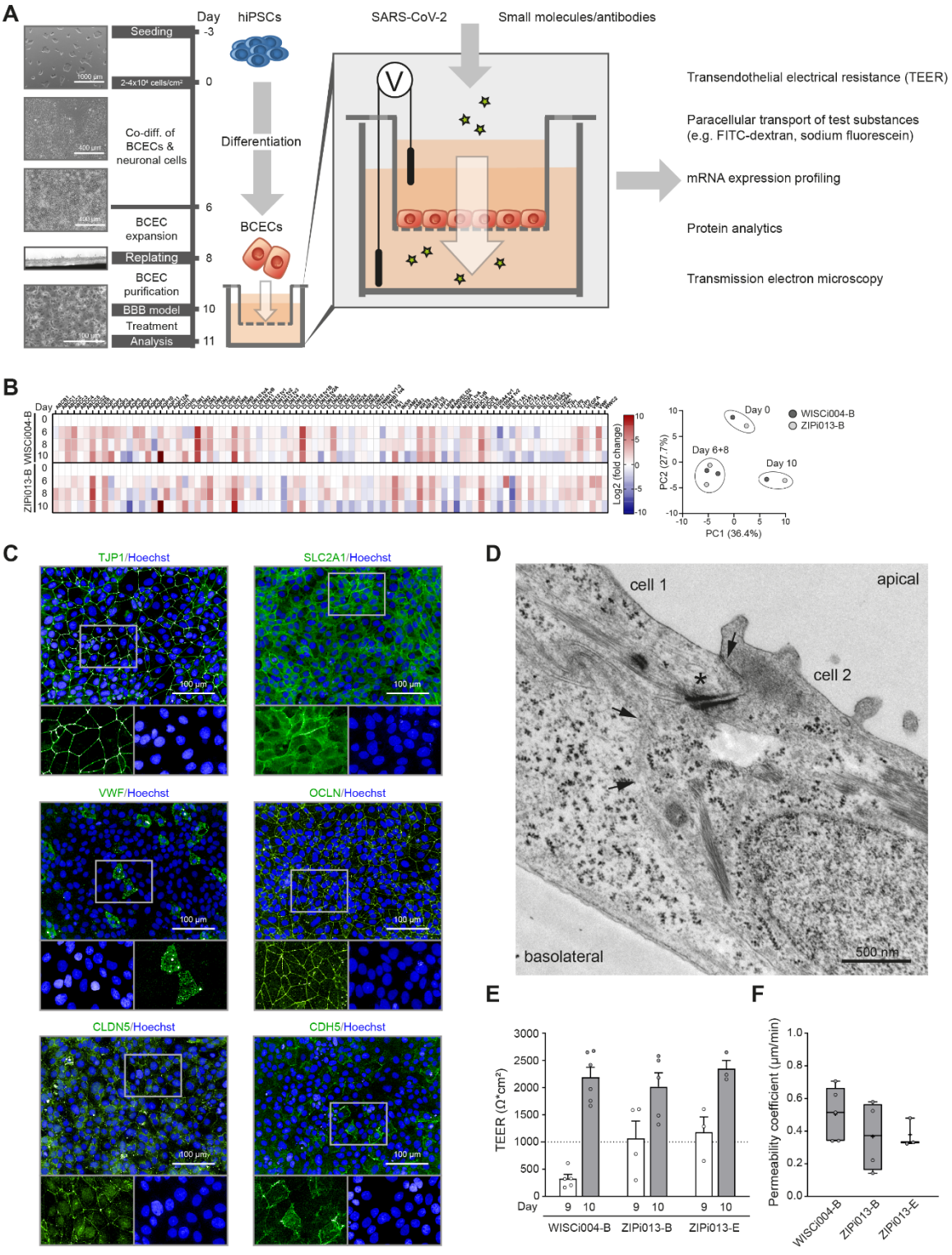

SI Figure 2: hiPS-derived brain capillary endothelial-like cell transwell model. (A) Schematic representation of the transwell model. After 10 days of differentiation, the size of hiPS-BCECs was increased compared to the donor hiPSCs and cells grew in close contact forming a confluent monolayer. **(B)** Expression of key BCEC marker genes during the course of differentiation, in particular tight junction (TJ) proteins (claudins, occludin), junction adhesion molecules (JAMs), adherence junction (AJ) proteins, solute carriers and efflux transporters. hiPS-BCECs derived from hiPSC lines WISCi004-B or ZIPi013-B show an increased expression of several of these transcripts. Respective time points are plotted (d=6, d=8, d=10) and were normalized to the respective hiPSC donor lines. In principle component analysis (PCA) the samples cluster according to the differentiation stage, indicating the

robustness of the differentiation protocol. **(C)** Expression of BCEC-specific marker proteins (TJP1, SLC2A1, VWF, OCLN, CLDN5, CDH5) after day 10 of the differentiation procedure (green). Nuclei stained with Hoechst 33258 (blue). Scale bars as indicated. **(D)** Transmission electron microscopy images of hiPS-BCECs. Neighboring cells are connected by complex TJs constricting the paracellular space (black arrows). Furthermore, adhesion points (punctum adherens, black asterisk in d) anchored within the actin filament network were detected, indicating the integrity of cell-cell contacts. Scale bars as indicated. **(E)** At day 9, TEER values were ~300 $\Omega*cm^2$, but at day 10 increased drastically to values of ~2000 $\Omega*cm^2$, a typical increase in barrier integrity and formation of associated TJ structures around that time. For all experiments of this study, only inserts with TEER values > 1000 $\Omega*cm^2$ were considered. Mean ± SEM of at least three independent biological experiments, at least three technical replicates each. **(F)** To characterize the size-dependent paracellular permeability of the BBB models, which is functionally linked to the expression of junctional molecules, especially of claudins, transport studies with the paracellular marker fluorescein (~0.33 kDa) were conducted. Fluorescein permeated very similarly in BBB models derived from three independent hiPSC lines (WISCi004-B, ZIPi013-B, ZIPi013-E). Mean ± SEM of at least three independent biological experiments, at least three technical replicates each.

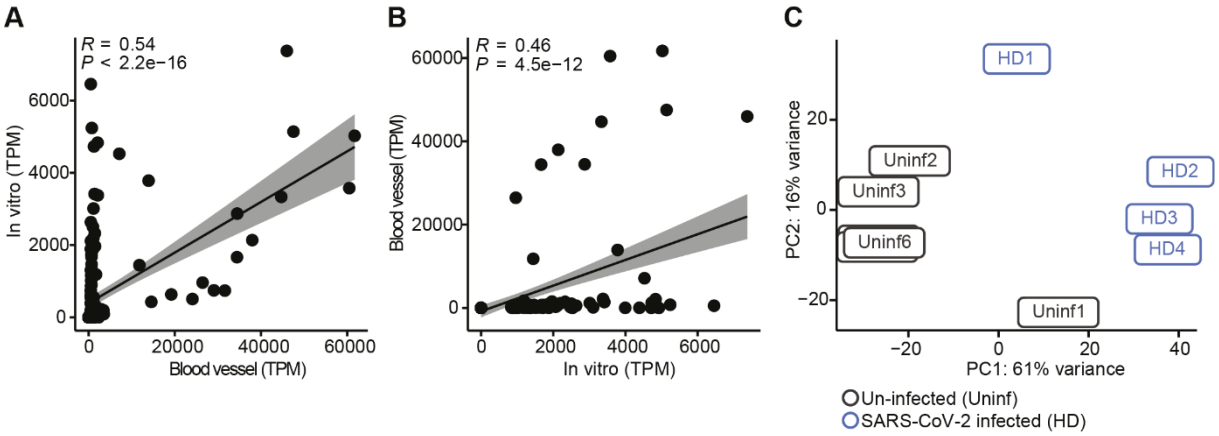

SI Figure 3: Transcriptional correlation of human cortical blood vessels with hiPS-BCECs. (A) Correlation of highest 100 and lowest 100 genes of hiPS-BCECs with respective genes in human cortical blood vessels. Normally distributed Pearson correlation was used. $R = 0.54$, $P < 2.2e\text{-}16$. **(B)** Correlation of highest 100 and lowest 100 genes of human blood vessels with respective genes in hiPS-BCECs. Normally distributed Pearson correlation was used. $R = 0.46$, $P = 4.5e\text{-}12$. **(C)** Principal component analysis of un-infected (n = 6) and SARS-CoV-2 infected hiPS-BCECs (n = 4). TPM: Transcripts per million.

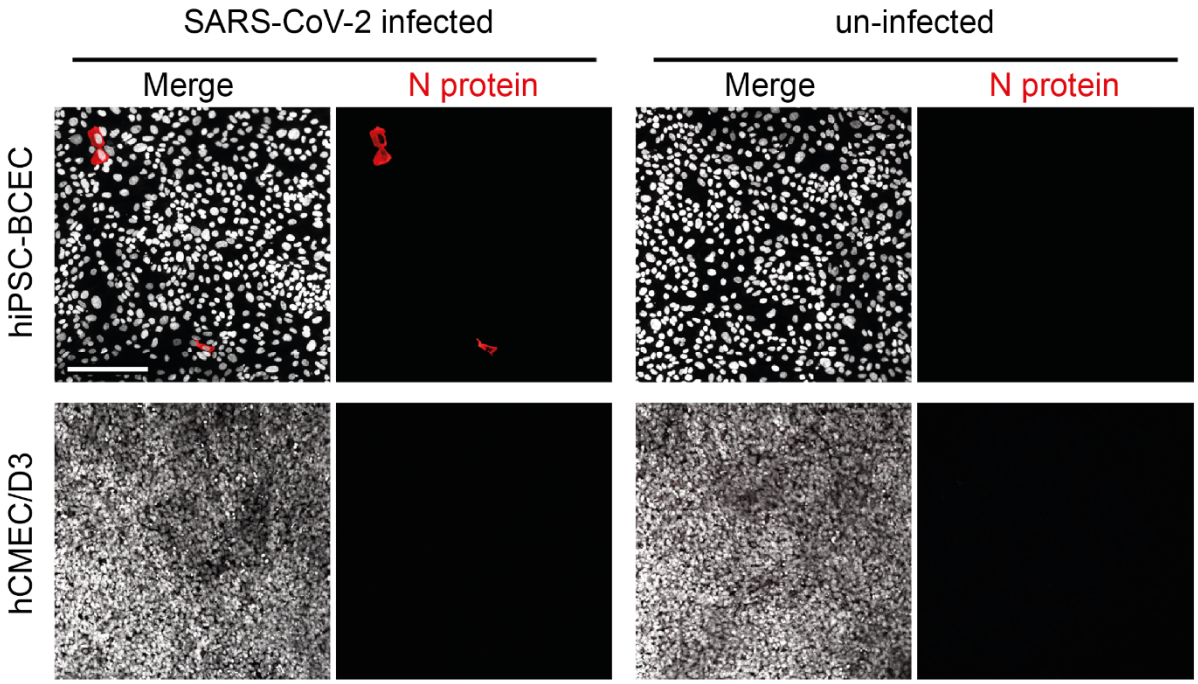

SI Figure 4: SARS-CoV-2 infection of hiPSC-BCECs and hCMEC/D3 in parallel. **Top row**: Representative images of infected/un-infected hiPSC-BCECs differentiated from WISCi004-B (IMR90-4). SARS-CoV-2 N protein staining (red), nuclei stained with DAPI (white). **Bottom row**: Representative images of infected/un-infected hCMEC/D3. SARS-CoV-2 N protein staining (red), nuclei stained with DAPI (white). Despite higher cell counts, not a single SARS-CoV-2 N protein positive hCMEC/D3 cell was observed after inf ection with an MOI of 10 in 4 independent wells (area 21.6 x 11.4 mm^2 each). Scale bar: 200 µm.

Supplemental table

SI Table 1: Epidemiological and clinical features of COVID-19 patients and controls.

Age (years)	Sex	Body mass index, kg/m^2	Place of death	Post mortem interval (days)	Disease course (days)	Cause of death	SARS-CoV-2 qPCR (brain)	Comorbidities	Mechanical ventilation
76 #	m	37.7	Intensive care unit	3	23	Sepsis	+	Adipositas, AML, DCM, S/P thyroid cancer	y
86 #	f	30.5	Hospital ward	3	10	Pneumonia	n.d.	Adipositas, atrial fibrillation, CHD, CKD, dementia, myelodysplastic syndrome	n
67 #	m	33.5	Hospital ward	2	2	Pneumonia, circulating distrubances in inflammation	n.d.	Adipositas, AH, DCM, lung emphysema, PD, schizophrenia, Type II diabetes	n
66	m	25.3	Emergency room	2	n.d.	Pneumonia	+	CHD, Type II diabetes	n
82	f	15.4	Hospital ward	4	5	Bronchitis	+	COPD, CKD, S/P PE	n
77	m	19.4	Hospital ward	2	29	Pneumonia	+	Atrial fibrillation, aortic aneurysm, cardiac hypertrophy, CKD, lung emphysema	n
85 #	f	18.1	Hospital ward	0	20	Pneumonia	+	Atrial fibrillation, cardiac insufficiency, CHD, CKD, myelofibrosis	n
51	m	20.7	Home	8	P. m. diagnosis	Pneumonia	n.d.	Liver cirrhosis	n
87	f	16.4	Hospital ward	3	2	Pneumonia, sepsis	n.d.	Colon cancer, emphysema, paranoid schizophrenia	n
76	f	21.7	Hospital ward	2	6	Pneumonia	n.d.	AH, breast cancer	n
59	f	ND	Intensive care unit	1	18	Pneumonia	+	Multiple myeloma	y
78 #	m	25.5	Home	2	P.m. diagnosis	Myocardial infarction	n.d.	AH, cardiac insufficiency, CHD, emphysema, liver cirrhosis	n
89 #	f	17.8	Hospital ward	2	1	Pneumonia	n.d.	Atrial fibrillation, CHD, S/P myocardial infarction	n

29 #	m	25.5	Work	6	2	Bronchopneumonia	n.d.	Cardiac hypertrophy, steatosis hepatis	n
46 #	f	n.d.	Home	1	No COVID-19	Myocardial infarction	-	n.d.	n
79	m	n.d.	n.d.	3	No COVID-19	Septic shock	-	n.d.	n
90	f	n.d.	n.d.	8	No COVID-19	Haemorrhagic shock	-	n.d.	n
92	m	n.d.	n.d.	13	No COVID-19	Heart failure	-	n.d.	n
66 #	f	n.d.	n.a.	Biopsy	No COVID-19	n.a.	-	Surgery for temporal lobe epilepsy	n
70 §	f	n.d.	n.a.	Biopsy	No COVID-19	n.a.	-	Surgery for temporal lobe epilepsy	n
62 #	m	n.d.	n.a.	Biopsy	No COVID-19	n.a.	-	Surgery for temporal lobe epilepsy	n
47 #	m	n.d.	n.a.	Biopsy	No COVID-19	n.a.	-	Surgery for temporal lobe epilepsy	n
37 §	m	n.d.	n.a.	Biopsy	No COVID-19	n.a.	-	Surgery for temporal lobe epilepsy	n
65 # §	f	n.d.	n.a.	Biopsy	No COVID-19	n.a.	-	Surgery for temporal lobe epilepsy	n

Abbreviations: m, male; f, female; AML, acute myeloleukaemia; DCM, dilated cardiomyopathy; S/P, status post; CHD, coronary heart disease; CKD, chronic kidney disease; AH, arterial hypertension; PD, Parkinson's Disease; COPD, chronic obstructive pulmonary disease; PE, pulmonary embolism; y, yes; n, no; # samples used for Nanostring DSP; § samples used for vessel isolation and RNA-seq; n.d. not determined; n.a. not applicable

Supplemental experimental procedures

Human induced pluripotent stem cells

We maintained human iPSCs lines WISCi004-B (Kadari et al., 2014), ZIPi013-B and ZIPi013-E (Tandon et al., 2018) in mTeSR™1 (#05850, mTeSR™1 Complete Kit, STEMCELL Technologies) under feeder-free conditions on Matrigel™ (Corning) coated multiwell plates at 37 °C with 5% CO_2. Cells were passaged at 70-80% confluency via incubation with Gentle Cell Dissociation Reagent (#07174, STEMCELL Technologies,) for 7 min at room temperature. Gentle Cell Dissociation Reagent was aspired, 1 ml mTeSR™1 was added and colonies were detached by scraping with a cell scraper. Cell aggregates were pipetted up and down in order to dissociate the colonies and seeded in fresh mTeSR™1 onto newly Matrigel™-coated plates in a 1:10-1:60 split ratio. Medium was exchanged on a daily basis.

hiPS-BCEC differentiation and establishment of the *in vitro* BBB model

For the infection model, we used the hiPSC line WISCi004-B/IMR90-4 (Kadari et al., 2014), but have also validated the model using hiPSC lines ZIPi013-B and ZIPi013-E (Tandon et al., 2018). WISCi004-B was extensively characterized by staining and quantifying pluripotency-associated markers, including OCT3/4, NANOG, SOX-2, LIN28 and CMYC, ScoreCard (Bock et al., 2011; Tsankov et al., 2015) and PluriTest analysis (Muller et al., 2011), which all passed. Initially, a single cell suspension of hiPSCs was prepared with Accutase (#A1110501, ThermoFisher Scientific). The cell suspension was centrifuged at 300 x g for 5 min and cells were seeded in mTeSR™1 supplemented with 10 µM Y-27632 (#72304, STEMCELL Technologies) onto Matrigel-coated 6-well plates (Nunc™, #140675, ThermoFisher Scientific). The seeding density was optimized for each hiPSC line. For the differentiation of hiPSCs to BCECs, the neurodevelopmental process *in vivo* has to be recapitulated *in vitro*. For brain-capillary endothelial-like cells, a co-differentiation of neural and endothelial cells was initiated by treatment with so-called unconditioned medium (Lippmann et al., 2014). After 2-3 days

when optimal cell densities of 2-4x10^4 cells/cm^2 were reached, medium was switched to unconditioned medium in order to initiate co-differentiation of BCECs and neuronal cells (referred to as day 0 of differentiation throughout the manuscript). Unconditioned medium was composed of 78.5% DMEM/F12 (#21331046, ThermoFisher Scientific), 20% KnockOut™ serum replacement (#10828028, ThermoFisher Scientific), 1% MEM NEAA (#1114050, ThermoFisher Scientific), 0.5% L-glutamine (#GLN-B, Capricorn), and 0.1 mM β-mercaptoethanol (#21985023, ThermoFisher Scientific). A daily change of unconditioned medium for 5 days was followed by double feeding at day 6 with endothelial cell (EC) medium supplemented with 20 ng/ml hbFGF (#D100-18B, Peprotech) and 10 µM retinoic acid (RA, #722262, STEMCELL Technologies) to expand the BCECs. EC medium was composed of Human Endothelial-SFM (#11111044, ThermoFisher Scientific) and, if not stated otherwise, 0.5% B27 Supplement (#17504044, ThermoFisher Scientific) as described recently (Neal et al., 2019). After 48 h without medium change, cells were dissociated with Accutase for 30 min and seeded at a cell density of 1x10^6 cells/cm^2 onto collagen IV/fibronectin-coated transwell inserts (#662-641, Greiner) in EC medium supplemented with 20 ng/mL hFGF and 10 µM RA. This seeding step at day 8 in combination with the collagen IV/fibronectin-coating allows for an efficient purification of BCECs. At day 9, hiPS-BCECs were adapted to EC medium without hFGF and RA (in transwell systems with 200 µl of medium apical and 800 µl basolateral) for 24 h. TEER measurements were performed to evaluate the integrity of the generated *in vitro* BBB to be used for further applications.

cDNA synthesis and low-volume qPCR for hiPS-BCEC characterization

These experiments were conducted as described previously (Ramme et al., 2019). For high-throughput qPCR, cells were harvested and total RNA was extracted according to the manufacturer's instructions using the NucleoSpin® RNA Kit (#740955.250, Macherey-Nagel). RNA concentration and quality was determined using a NanoDrop™ 1000 Spectrophotometer (ThermoFisher Scientific) and samples were stored at -80 °C until further use. A total volume

of 20 µl cDNA was synthesized from 250 ng of RNA using the High Capacity cDNA Reverse Transcriptase Kit (#4368814, Thermo Fisher Scientific). Targets were preamplified in order to increase the concentration of the targets and reduce required input sample volume. For preamplification the tenfold concentration of gene targeting primers was used in combination with Qiagen Mastermix and HotStar Plus Taq Polymerase (#203603, Qiagen). The high-throughput qPCR was performed with the preamplified cDNA in 96 samples × 96 targets chips using the Biomark™ System (Fluidigm®). The following 90 targets were investigated (claudin nomenclature according to (Mineta et al., 2011)): *ABCB1*, *ABCC1*, *ABCC2*, *ABCC3*, *ABCC4*, *ABCC5*, *ABCG2*, *AGER*, *AQP1*, *AQP2*, *AQP3*, *AQP4*, *AQP5*, *AQP6*, *AQP7*, *AQP8*, *AQP9*, *AQP10*, *AQP11*, *AQP12A*, *CDH1*, *CDH5*, *CLDN1*, *CLDN2*, *CLDN3*, *CLDN4*, *CLDN5*, *CLDN6*, *CLDN7*, *CLDN8*, *CLDN9*, *CLDN10 tva*, *CLDN10 tvb*, *CLDN11*, *CLDN12 tv1*, *CLDN12 tv2*, *CLDN12 tv3*, *CLDN14*, *CLDN15*, *CLDN16*, *CLDN17*, *CLDN18 tv1b*, *CLDN18 tv2a*, *CLDN19*, *CLDN20*, *CLDN21*, *CLDN22*, *CLDN23*, *CLDN24*, *CLDN25, CLDN26*, *CLDN27*, *CTNNB1 tv1-3*, *CTNNB1 tv4*, *F11R*, *FN1*, *INSR*, *JAM2*, *JAM3*, *KRT8*, *KRT18*, *KRT19*, *LRP1*, *LRP8*, *MARVELD2*, *MFSD2A*, *MUC1 tva*, *MUC1 tvb*, *MUC18*, *MUC20*, *OCLN*, *S100A4 tv1*, *S100A4 tv2*, *SELE*, *SLC1A1*, *SLC2A1*, *SLC7A1*, *SLC7A3*, *SLC7A5*, *SLC16A1*, *SLC16A2*, *SLC29A1*, *TFRC*, *TJP1*, *TJP2*, *TJP3*, *VEGFA*, *VIM*, *VWF*, *WWC2*. Threshold cycle (C_t) values were normalized to the endogenous housekeeping genes *PPIA*, *ACTB*, *GAPDH* and *B2M* and relative quantification was performed based on the comparative $2^{-\Delta Ct}$ method. Differential gene expression was visualized in a heatmap of the $\log_2$-fold change normalized to the respective hiPSC donor lines or with the two principle components obtained from PCA, which explain most of total variance.

Immunofluorescent staining of the SARS-CoV-2-infected or un-infected hiPS-BCEC monolayer and image analysis

hiPSC-derived BCECs were grown in 96-well imaging plates (#655-866, Greiner) or on transwell inserts (#662-641, Greiner) and fixed for 10 min in 4% formaldehyde. SARS-CoV-2

infected BCECs were soaked in formalin for 24 h. After washing with PBS, cells were permeabilized with 0.1-0.2% Triton X-100 in PBS. After additional washing, cells were blocked with 3% BSA and 0.1% Tween 20 in PBS or Blocking Medium (#15252, Active Motif). Primary antibodies were diluted in blocking solution and incubated overnight at 4 °C. The following antibodies and dilutions were applied: anti-TJP1/ZO-1 (1:400, #21773-1-AP, Proteintech), anti-SLC2A1/GLUT-1 (1:200, #ab115730, Abcam), anti-VWF (1:50, #555849, BD Pharmingen), anti-OCLN (1:200, #33-1500, ThermoFisher Scientific), anti-CLDN5 (1:100, #ab15106, Abcam), anti-CDH5 (1:100, # sc-9989, Santa Cruz Biotechnology), anti-spike (1:300; #GTX632604, GeneTex), anti-N (1:1000; #40143-T62, Sino Biological or 1:1000; #HS-452011, Synaptic Systems) and anti-dsRNA (1:200; #Ab01299-23.0; absolute antibody; rabbit monoclonal antibody of J2-anti-dsRNA antibody). Cells were thoroughly washed and then incubated with secondary antibodies (1:500, Alexa Fluor® 488/555/647 antibodies, ThermoFisher Scientific) diluted in blocking solution for 1-1.5 h at room temperature in the dark. Cells were then washed twice with PBS and nuclear counterstaining was performed for 15 min with 1 µg/ml Hoechst 33258 (#H3569, Invitrogen) or DAPI (#10184322, ThermoFisher Scientific), followed by two additional washing steps. Cells on 96-well imaging plates were imaged using the Opera or Operetta High Content Imaging System (PerkinElmer). The image analysis and quantification of the pluripotency-associated markers was performed using the Columbus™ Image Data Storage and Analysis system (PerkinElmer). Transwell insert membranes were carefully cut out and mounted upside down on glass slides (ibidi µ-Slide #80287) for confocal microscopy. These were imaged with a Leica SP5 confocal microscope and a 20x oil or 63x oil objective. Three random pictures were acquired with a size of 600,000 μm^2 per condition. 20x images were processed by ImageJ to determine the number of SARS-CoV-2 protein positive cells in relation to all DAPI-positive nuclei.

Fluorescein transport

Permeation of fluorescein across the established *in vitro* BBB model was measured to study the paracellular transport capacity and thus the tightness of the BBB. Fluorescein sodium salt (#F6377, Sigma-Aldrich) was dissolved in EC medium to a final concentration of 10 µM. The apical medium from all transwell inserts to be examined, including inserts containing cells (BBB model) and empty inserts (blanks), was replaced by 200 µl fluorescein solution. Immediately after, the inserts were transferred to a new 24-well plate containing 800 µl of fresh EC medium and placed for 1 h in the incubator at 37 °C and 5% CO_2. To assess fluorescence intensity, samples from both, apical and basolateral compartments, the 10 µM fluorescein starting solution and pure EC medium were pipetted into a 96-well plate (#655-900, Greiner). The concentration of the fluorescent tracer molecule in each sample was measured using a fluorescence plate reader (Infinite M1000 Pro, TECAN, excitation: 490 nm, emission: 525 nm) and the permeability coefficients were calculated as described previously (Neuhaus et al., 2008). In case of SARS-CoV-2 infection experiments, samples were mixed 1:1 with a buffer containing ≤ 40% guanidinie hydrochloride in Tris-HCl (Roche media kit, Roche) for inactivation prior to fluorescence intensity measurements.

Transendothelial electrical resistance (TEER) measurements

To evaluate the tightness and integrity of the generated *in vitro* BBB, the TEER across the hiPS-BCEC monolayer was measured in real-time without damaging the cells. To this end, alternating electrical signals were applied using electrodes placed on both sides of monolayer and the resulting voltage and current are used to calculate the electrical resistance in $\Omega*cm^2$. TEER values were measured using the Millicell®-ER system (#MERS00002, Merck Millipore) in combination with the STX01 electrode (Merck Millipore). Prior to the measurement, the electrode was placed in 70% ethanol for 10 min, then dipped into sterile H_2O and equilibrated in EC medium for at least 15 min. A test electrode (#STX04, Merck Millipore) was used to control and adjust the TEER instrument if necessary. The TEER measurements were performed 40 min after medium exchange. The 24-well plates containing the transwell inserts

were placed on an aluminium spacer plate positioned on a heating plate set to 37 °C and subsequently, the resistance was measured in both empty (blank) and cell containing inserts (BBB model) at three different positions of the insert membrane. TEER values were calculated based on the following formula:

$$TEER\ [\Omega * cm^2] = (R_{BBB\ model} - R_{blank})\ [\Omega] * A\ [cm^2]$$

R = resistance

A = culture area of the transwell insert

Transmission electron microscopy (TEM)

hiPS-BCECs were fixed with 1% glutaraldehyde and 4% paraformaldehyde in 0.1 M PBS, pH 7.2 overnight. Cells were washed three times with PBS, rinsed three times in 0.1 M sodium cacodylate buffer (pH 7.2-7.4) and osmicated using 1% osmium tetroxide in cacodylate buffer. Following osmication, the sections were dehydrated using ascending ethyl alcohol concentration steps, followed by two rinses in propylene oxide. Infiltration of the embedding medium was performed by immersing the samples in a 1:1 mixture of propylene oxide and Epon and finally in neat Epon. Polymerization was carried out at 60 °C. Semithin sections (0.5 µm) of cross-sections of hiPS-BCEC transwell cultures were prepared for light microscopy by staining for 1 minute with 1% Toluidine blue and mounting on glass slides. Ultrathin sections (60 nm) were examined in an EM902 (Zeiss). Pictures were acquired with a TRS 2K digital camera (A. Tröndle).

Isolation of human brain vessels

Human brain vessels were isolated as previously described (Lee et al., 2019). Briefly, fresh cortex tissue from a brain biopsy was homogenized in 1 ml MCDB131 medium (ThermoFischer Scientific) using a dounce homogenizer, further diluted in medium, and centrifuged (4 °C) at

2000 g for 5 min. The pellet was resuspended in 15% (wt/vol) 70 kDa dextran and centrifuged (4 °C) for 15 min at 10000 g. The microvessel containing pellet was retrieved and transferred to a 40 µm cell strainer. After washing with PBS, the microvessels were placed in 0.5% BSA/MCDB131 medium and centrifuged (4 °C) for 10 min at 5000 g. The final pellet was resolved in RNA isolation buffer and stored at -80 °C for further applications.

Immunohistochemical staining and analysis of human cortex tissue

Brain tissue was fixed in 4% buffered formalin and processed for paraffin embedding. Sections were cut (2 µm) and mounted. After dewaxing and inactivation of endogenous peroxidases (3% hydrogen peroxide), antibody-specific antigen retrieval was performed. Antibodies used in our study were anti-ACE2 (1:100; #AF933; R&D Systems), anti-NRP1 (1:500; #MBS178289, MyBiosource), anti-IFITM2 (1:3000; #MA5-27503, Invitrogen) and anti-CD31/PECAM1 (1:50; #HPA004690; Atlas Antibodies). Immunohistochemical staining were performed using a Ventana benchmark XT autostainer (Ventana). For detection of specific binding, the Ultra View Universal DAB Detection Kit (Ventana, Roche) was used which contains secondary antibodies, DAB stain, and counterstaining reagent for detection of nuclei. Slides were examined by experienced morphologists and representative pictures were taken with a Leica DMD108 digital microscope. For the quantification of specific signal, stained human cortex sections were scanned using a Hamamatsu NanoZoomer automatic digital slide scanner (Hamamatsu Photonics, Hamamatsu, Japan) and images of whole stained sections were obtained at a resolution of at least 1 pixel per µm. CD31 signals were assessed using ImageJ Software (version 1.52p, NIH, Bethesda, MA, USA). The plugin “colour deconvolution” and the H&E vectors were used to separate the channels (Ruifrok and Johnston, 2001). The brown channel with the RGB values (R: 0.26814753, G: 0.57031375, B: 0.77642715) was used. After applying the automatic threshold, the “analyze particles” script was used to measure the CD31 signal. Measurements included the area, standard deviation, min and max grey value, mean grey

value, shape descriptions and integrated density. The signal of the total tissue was measured to derive a portion of area covered by CD31.

hCMEC/D3 cultivation

hCMEC/D3 were cultured according to published protocols (Forster et al., 2008).

PluriTest analysis

For PluriTest analysis, RNA was isolated using the RNeasy Mini Kit (#74104, Qiagen) with an optional on-column DNase Digestion step (RNase-Free DNase Set, #79254, Qiagen). For microarray analysis, 200-500 ng of total RNA were amplified and biotinylated using the TargetAmp™ - Nano Labeling Kit for Illumina® Expression BeadChip (#TAN07924, Illumina). Concentration of Biotin-aRNA was measured with a Qubit 3.0 Fluorometer (Thermo Fisher Scientific) and the concentration of each sample was adjusted to 150 ng/µl. 750 ng of Biotin-aRNA were used for hybridization with the HumanHT-12 v4.0 Expression BeadChip (#BD-103-0604, Illumina) and hybridization was performed at 58 °C for 16-20 h. After hybridization, BeadChips were washed and stained according to the manufacturer's standard protocol. BeadChips were scanned using the iScan instrument (Illumina). Raw data (*.idat files) were submitted to PluriTest analysis at www.pluritest.org (Muller et al., 2011).

ScoreCard

ScoreCard assays were performed following the procedures outlined in the original publication (Tsankov et al., 2015).

Supplemental references

Bock, C., Kiskinis, E., Verstappen, G., Gu, H., Boulting, G., Smith, Z.D., Ziller, M., Croft, G.F., Amoroso, M.W., Oakley, D.H., et al. (2011). Reference Maps of human ES and iPS cell variation enable high-throughput characterization of pluripotent cell lines. Cell *144*, 439-452.

Forster, C., Burek, M., Romero, I.A., Weksler, B., Couraud, P.O., and Drenckhahn, D. (2008). Differential effects of hydrocortisone and TNFalpha on tight junction proteins in an in vitro model of the human blood-brain barrier. J Physiol *586*, 1937-1949.

Kadari, A., Lu, M., Li, M., Sekaran, T., Thummer, R.P., Guyette, N., Chu, V., and Edenhofer, F. (2014). Excision of viral reprogramming cassettes by Cre protein transduction enables rapid, robust and efficient derivation of transgene-free human induced pluripotent stem cells. Stem Cell Res Ther *5*, 47.

Lee, Y.K., Uchida, H., Smith, H., Ito, A., and Sanchez, T. (2019). The isolation and molecular characterization of cerebral microvessels. Nat Protoc *14*, 3059-3081.

Lippmann, E.S., Al-Ahmad, A., Azarin, S.M., Palecek, S.P., and Shusta, E.V. (2014). A retinoic acid-enhanced, multicellular human blood-brain barrier model derived from stem cell sources. Sci Rep *4*, 4160.

Mineta, K., Yamamoto, Y., Yamazaki, Y., Tanaka, H., Tada, Y., Saito, K., Tamura, A., Igarashi, M., Endo, T., Takeuchi, K., and Tsukita, S. (2011). Predicted expansion of the claudin multigene family. FEBS Lett *585*, 606-612.

Muller, F.J., Schuldt, B.M., Williams, R., Mason, D., Altun, G., Papapetrou, E.P., Danner, S., Goldmann, J.E., Herbst, A., Schmidt, N.O., et al. (2011). A bioinformatic assay for pluripotency in human cells. Nat Methods *8*, 315-317.

Neal, E.H., Marinelli, N.A., Shi, Y., McClatchey, P.M., Balotin, K.M., Gullett, D.R., Hagerla, K.A., Bowman, A.B., Ess, K.C., Wikswo, J.P., and Lippmann, E.S. (2019). A Simplified, Fully Defined Differentiation Scheme for Producing Blood-Brain Barrier Endothelial Cells from Human iPSCs. Stem Cell Reports *12*, 1380-1388.

Neuhaus, W., Plattner, V.E., Wirth, M., Germann, B., Lachmann, B., Gabor, F., and Noe, C.R. (2008). Validation of in vitro cell culture models of the blood-brain barrier: tightness characterization of two promising cell lines. J Pharm Sci *97*, 5158-5175.

Ramme, A.P., Koenig, L., Hasenberg, T., Schwenk, C., Magauer, C., Faust, D., Lorenz, A.K., Krebs, A.C., Drewell, C., Schirrmann, K., et al. (2019). Autologous induced pluripotent stem cell-derived four-organ-chip. Future Sci OA *5*, FSO413.

Ruifrok, A.C., and Johnston, D.A. (2001). Quantification of histochemical staining by color deconvolution. Anal Quant Cytol Histol *23*, 291-299.

Tandon, R., Brandl, B., Baryshnikova, N., Landshammer, A., Steenpass, L., Keminer, O., Pless, O., and Muller, F.J. (2018). Generation of two human isogenic iPSC lines from fetal dermal fibroblasts. Stem Cell Res *33*, 120-124.

Tsankov, A.M., Akopian, V., Pop, R., Chetty, S., Gifford, C.A., Daheron, L., Tsankova, N.M., and Meissner, A. (2015). A qPCR ScoreCard quantifies the differentiation potential of human pluripotent stem cells. Nat Biotechnol *33*, 1182-1192.